JOURNAL OF SOLID STATE CHEMISTRY 45, 399–410 (1982)

Electronic Influences on the Crystal Chemistry of Transition Metal–Main Group *MX* and MX_2 Compounds

JEREMY K. BURDETT

Department of Chemistry, The University of Chicago, Chicago, Illinois 60637

Received April 28, 1982; in final form July 21, 1982

It is shown how (a) the number of electrons per formula unit and (b) the energy difference between the transition metal *d* orbitals and the main group element *s,p* orbitals are of paramount importance in determining the crystal structures of *MX* and MX_2 systems. The occurrence of some fifty diverse structural types may be organized by using these two parameters.

Introduction

The solid-state structures of compounds formed between a transition metal (*M*) and a main group element to its right in the periodic table (*X*) display an extremely wide spectrum of geometrical arrangements (*1–4*) of stoichiometry *MX* and MX_2. These range from the "typically ionic" structures of the CaF_2 and rutile TiO_2 types found for many dioxides through the densely packed structure of $HfGa_2$ to the "typically alloy-like" structure of $CuAl_2$ found for several stannides and plumbides. In order to be able to understand these tremendous variations in structural properties, we will eventually need to probe their electronic structure by numerical calculation of a large number of systems with different electron counts and composition. A start has been made in the sense that many calculations are available (*5*) on individual or small groups of compounds. Not all, however, were aimed at understanding the occurrence of a particular geometry. It would be important to introduce some systemization into the structures of this diverse collection of materials. One technique which has been found to be extremely useful in this area, and which we will use here, is that of structural mapping (*6–18*). Very often a plot of $\xi_1(A,B)$ versus $\xi_2(A,B)$ for all AB_n compounds with a given stoichiometry and perhaps total electron count leads to regions in such a two-dimensional display where examples of one structure are topologically separated from examples of another. $\xi_{1,2}$ are indices which are ultimately related to parameters which depend upon the location (in terms of row and column number) of each element in the periodic table. For the *AB* octets, for example, $\xi_{1,2}$ might be the crystal radii r_+,r_- of *A,B* (*16, 17*) or the sums of the pseudopotential *s* and *p* radii, r_σ^A and r_σ^B, or some combination of them (*6, 7, 10–18*). Mooser–Pearson diagrams (*1, 19*) use the mean value of the valence shell quantum number for ξ_1 and the Pauling electronegativity difference for ξ_2. Watson and Bennett's studies of transition metal–transition metal alloys (*9*) used two band-theoretically derived indices; an elec-

0022-4596/82/150399-12$02.00/0

tronegativity difference (via the work function) and the average number of d electron holes in the alloy band. All of these indices mentioned are of course related to each other, some in rather ill-defined ways perhaps. There is healthy competition for the generation of a set of atomic parameters which, when used with a judicious choice of indices, will lead to perfect (or near-perfect) structural sorting of a given data base. In this paper we will present structural maps for MX and MX_2 systems, which are not perfect by any means, but which identify important factors influencing the structures of these species, and allow geometrical trends to be followed.

Indices

One of our indices will be the total number of valence electrons per formula unit (N). This of course is an index independent of the row number of either M or X. The importance of the electron count in determining crystal or molecular structure is well known but has seldom been used to look at the set of compounds we study here. We developed these counting ideas further by showing how geometrical changes in series of solid-state structures may be understood as the response of a parent structure to the presence of extra electrons (*17, 20–22*). (Similar approaches have been used for molecules (*23*).) Basically the geometry distorts so as to primarily reduce the energy of electrons in fiercely antibonding orbitals and, to a lesser extent, to involve occupied nonbonding orbitals in bonding. In molecules the result is an increase in the HOMO–LUMO gap on distortion and in solids an increase in the band gaps as the lattice vectors move (*18*). In a previous study (*20*) we have shown how a subset of the present MX_2 structural problem can be viewed in this way by studying the geometrical–electronic relationships between the calcium carbide; pyrite, marcasite; rutile, fluorite, cadmium halide sequence.

Our other index measures the energy difference between the transition metal and main group valence energy levels. Out of the many possible ways to do this we chose a purely theoretical and purely atomic function $\Delta E = M(d) - \frac{1}{4}[X(s) + 3X(p)]$, i.e., the difference between the metal d orbital levels and the weighted average of the X-atom s and p levels. The energies for this purpose are calculated ones and come straight from the Hartree–Fock computations of Herman and Skillman (*24*). For the metal levels the result depends on the chosen electronic configuration $nd^x(n+1)s^y$. Figure 1 shows the variation in transition metal d orbital

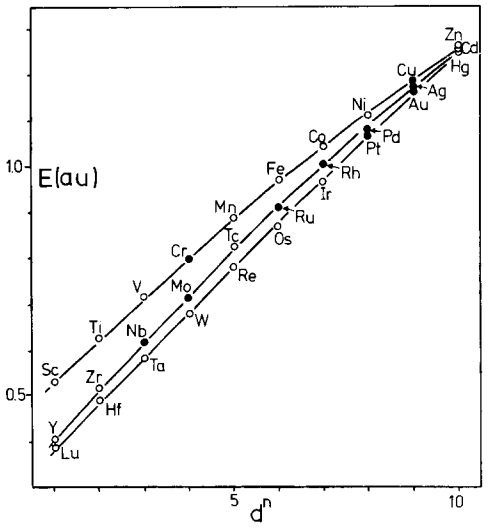

FIG. 1. d orbital energies from the Herman–Skillman computations (*24*) For $d^n s^2$ configurations (open circles); by interpolation (solid circles). For the ith row of the periodic table these curves are represented by a simple quadratic $E = \sum_{k=1}^{3} a_{ik} j^k$, where j runs from 1 (Sc group) to 10 (Cu group). The values of a_i for the three rows of the periodic table are $a_1 = 0.41985$, $a_2 = 0.10496$, $a_3 = -0.00235$ for the first row, $a_1 = 0.34617$, $a_2 = 0.10166$, $a_3 = -0.00114$ for the second row, and $a_1 = 0.29055$, $a_2 = 0.09916$, $a_3 = -0.00023$ for the third row.

energy for the $d^n s^2$ configuration where available and interpolated values for the missing data. For the set of MXX' species, included in the MX_2 data base, we used the average of the ΔE values for M/X and M/X'. Anticipating some of our later discussion, it is notable from this plot that many of the values cluster according to column number in the periodic table. A somewhat poorer resolution of structure is obtained if column number is used rather than our ΔE parameter, which includes a row and column number dependence. In the area of transition metal alloys there have been discussions (*14, 15*) concerning the value of such row-independent indices. Qualitative discussion concerning the occurrence of particular structure types in the literature often uses the column number (i.e., chemical group) as a useful label.

ΔE of course represents a simple electronegativity difference in the Mulliken sense between metal and nonmetal which may be estimated in many other different ways (*6–9*). In our study here we chose the very simplest set of indices taken from atomic data. Structure maps using ΔE and N as indices for MX_2 and MX systems are shown in Figs. 2 and 3, respectively. While neither are perfect, the majority of examples with a given structure fall within a well-defined area with very few rogue points lying far off. The data bases used are given in the Appendix.

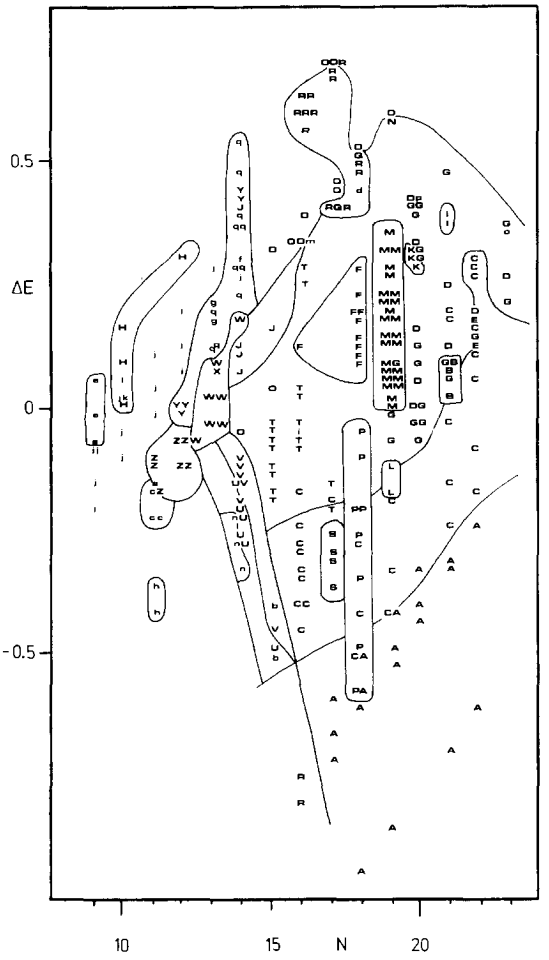

FIG. 2. Structure map for MX_2 systems. Key: A, rutile; B, $IrSe_2$; C, CdI_2; D, marcasite; E, PdS_2' F, löllingite; G, pyrite; H, $HfGa_2$; I, CuP_2; J, $MoSi_2$; K, PdP_2; L, ReS_2; M, FeAsS; N, $AuSn_2$, O, $CuAl_2$; P, MoS_2; Q, $PdSn_2$, $CoGe_2$, R, CaF_2; S, MoS_2 and CdI_2; T, $NbAs_2$; U, $PbCl_2$; V, $TiAs_2$; W, $CrSi_2$; X, $CuMg_2$; Y, $TiSi_2$; Z, $ZrSi_2$; a, $GdSi_2$; b, Cu_2Sb; c, $\alpha ThSi_2$; d, $CaCl_2$; e, Cu_2Mg; f, RuB_2; g, ReB_2; h, CaC_2; i, MoP_2; j, AlB_2; k, $MgZn_2$; l, $ZrGa_2$; m, $FeSi_2$; n, PbFCl; o, $AuTe_2$; p, $PdBi_2$; q, Nowotny chimney-ladder structures. Some of the points are coincident within the resolution of the map. These we have set side by side. In many cases the dividing line has been drawn to take advantage of this artificial separation purely by the prerogative of artistic license and not for any scientific deception. In addition, we have not been bound by straight lines, ellipses, or any other specific shape in drawing our boundary lines. These we have drawn solely to focus the reader's eye and help corral examples with the same structure.

The MX_2 Series

At the far left-hand side of the diagram, around $\Delta E \sim 0$, several examples of the Laves-phase structures Cu_2Mg and Zn_2Mg types are found. These are traditionally regarded as arising via efficient packing of spheres of different sizes. Further to the right, the structures of $ZrGa_2$ and $HfGa_2$ are found, which are superstructures based on close packings of both M and X components. As the number of electrons increases

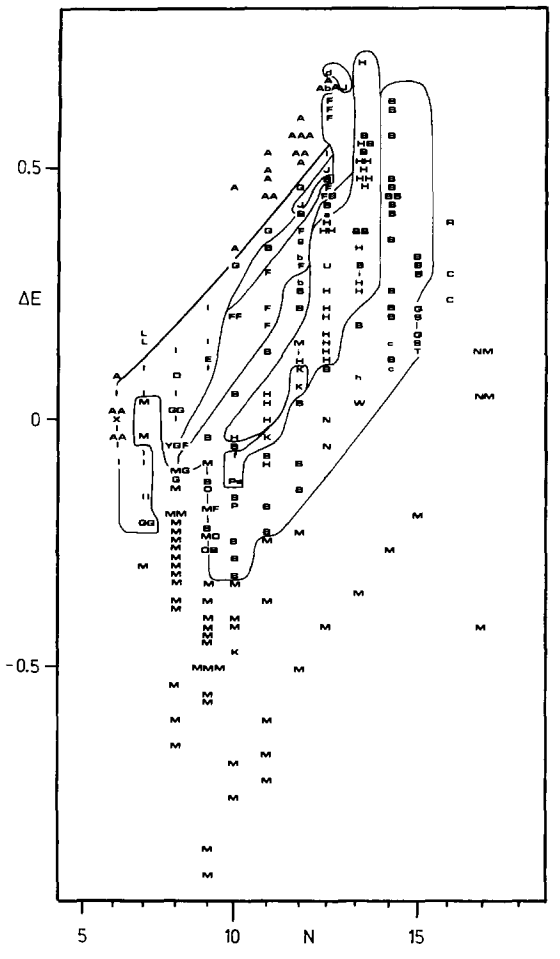

FIG. 3. Structure map for MX systems. Key: A, CsCl; B, NiAs; C, CuS; D, AuCd; E, NbPb; F, FeSi; G, FeB; H, MnP; I, CrB; J, CoSn; K, MoP; L, CuAu; M, NaCl; N, ZnS; O, TiAs; P, NbAs; Q, NiS; R, CuTe; S, PdS; T, PtS; U, $InNi_2$; V, CoGe; W, PbO; X, CrB and CsCl; Y, CrB and FeB; Z, NaCl and TiAs; a, MnP, FeSi, CsCl; b, FeSi, CsCl; c, NiS, NiAs; d, CsCl, CoSn; e, NaCl, MoP; F, NaCl, MoP, TiAs; g, CoSn, FeSi; h, NiAs, PbO; i, MnP, NiAs; j, NiAs, NaCl; k, MnP, FeSi. Some of the points are coincident within the resolution of the map. These we have set side by side. In many cases the dividing line has been drawn to take advantage of this artificial separation purely by the prerogative of artistic license and not for any scientific deception. In addition, we have not been bound by straight lines, ellipses, or any other specific shape in drawing our boundary lines. These we have drawn solely to focus the reader's eye and help corral examples with the same structure.

less compact structures are found. First, the closely related group of $MoSi_2$, $CrSi_2$, and $TiSi_2$ structural types are cleanly resolved. These consist of close-packed planes of MX_2 stoichiometry stacked, not as a close packing, but in the *bcc* (110) stacking pattern. The three structure types just mentioned are simply polytypes which differ in the stacking sequence. It is interesting that just the use of these two simple indices sorts them from one another. The $MoSi_2$ type (Strukturbericht symbol $C11_b$) is related to that of CaC_2 ($C11_a$). Both may be regarded as derived from rock salt by the substitution of the nonmetal by C_2 or Si_2 units lying parallel to 001. In $MoSi_2$ the Si–Si distance is long and these pairwise interactions are not of direct importance, but in CaC_2 discrete atom pairs are seen. Note that the $C11_a$, $C11_b$ regions are well separated on the map. The CaC_2 structure only occurs for systems with a large energy difference between an electropositive metal and carbon.

We included on this MX_2 map some examples of the fascinating Nowotny chimney-ladder phases. These are a whole family of closely related structures built up from the basic $TiSi_2$ arrangement, of general formula M_xY_y, where $1.25 \leq y/x < 2$. We calculated ΔE in the usual way but for our plot used as ordinate the total number of valence electrons in M_xY_y divided by x. A well-defined area is found containing these species which lies between approximately 13 and 14 electrons and which lies to higher ΔE values than the bulk of the $MoSi_2/CrSi_2/TiSi_2$ examples. Two species ($RuAl_2$ and $RuGa_2$) with the $TiSi_2$ structure itself are found in this region. The three examples with distorted AlB_2 structures (RuB_2 and ReB_2 types) are found in the same region.

The $ZrSi_2$ structure is a filled-up CrB type with trigonal prismatic coordination of the metal, a feature also of the AlB_2 and $ZrGa_2$ and $HfGa_2$ structures found adjacent to it. In $ZrSi_2$ there are zigzag chains involving

half of the Si atoms. In the AlB_2 structure there are graphite-like sheets of B atoms. Adjacent to both AlB_2 and $ZrSi_2$ regions are examples with the $GdSi_2$ and $\alpha ThSi_2$ structures (two very similar arrangements) which also contain triangular prisms of X atoms but this time linked together in a three-dimensional framework.

As the electron count increases, pairs, rather than chains or 3^6 nets of X atoms, become a feature of the structure. In the $NbAs_2$ structure half of the X atoms are paired up with each other. In the marcasite, pyrite, löllingite, and arsenopyrite structures, all the X atoms are present as pairs. It is interesting to see that while pyrite and marcasite examples (reached geometrically from CaC_2 by tilting the X_2 units so they point along 111 and related directions) are not resolved on our map, the distorted löllingite and arsenopyrite structures are separated from the parent, undistorted marcasites. (Parenthetically we note that in many cases, e.g., FeS_2, $FeSe_2$, pyrite and marcasite are very close in energy and both forms are known). Further to the right, anion polymerization proceeds beyond simple dimerization. In the CuP_2 structure, half of the phosphorus atoms are two coordinate and the other half three coordinate by other phosphorus atoms, in accord with simple valence rules. A three-dimensional framework is formed. (The structure contains Cu_2^{2+} units and is very similar to that of $Cd^{2+}P_4$.) The PdP_2 examples lie close by and consist of zigzag chains of phosphorus atoms with the square planar metal coordination typical of low-spin Pt^{II}, Pd^{II}. NiP_2 with this structure transforms to the pyrite structure under pressure.

At the bottom of the pyrite/marcasite region the CdI_2 and MoS_2 structural types are found. These contain no X–X pairs. It is interesting to note the boundary occurrence of the $IrSe_2$ structure, an arrangement somewhat between marcasite and rutile, where half of the atoms are found as pairs. Also in the boundary region we see the distorted CdI_2 structure found for ReS_2 and $ReSe_2$, where the cations have a tendency to pair up slightly and move away from the centers of the sulfur or selenium octahedra. The distorted pyrite structure of PdS_2 also lies at the edge of the pyrite structural field. From the map we see that the rutile structure itself is found for systems with a large negative level separation between M and X, and for systems with 17 electrons or more. With 16 electrons the fluorite structure is found, although the example with the larger ΔE (and therefore close to the CdI_2 and other structural regions) is ZrO_2, well known for its polymorphism. Note that the fluorite type actually occupies two distinctly different regions on the map, both of which occur for large MX electronegativity differences.

In a previous paper (20) we noted that structures containing chalconide dimers were invariably found when the sum of the third and fourth ionization potentials of the metal exceeded a certain critical value. Otherwise the MoS_2, CdI_2, or TiO_2 types were found which contained no dimers. This was understandable by consideration of the formal charges on the atoms in the two arrangements; $M^{2+}(X_2)^{2-}$ versus $M^{4+}(X^{2-})_2$ leading to a total of 14 X-located electrons when dimers are present and 16 X-located electrons when they are not. In the right-hand side of the diagram we qualitatively see a similar feature. At the top of the diagram, the points represent combinations with chalcogen of the more electronegative metal atoms, i.e., the ones with the deeper lying d orbitals. On moving down the diagram, the d orbital energy becomes smaller. It is interesting to see that a single "d orbital energy" is able to resolve the structures in the same way as before but with greater versatility (irrespective of the nature of X) than the ionization potential sum. In terms of stabilities of specific metal atom configurations, is it coincidental that

the $IrSe_2$ structure lies on the borderline? It is often suggested that this structure is stable because of the special stability of the low-spin d^6 Ir^{3+} configuration. (With half the X atoms linked as dimers and the other half present as free ions the species is formally written as $(Ir^{3+})_2(X_2)^{2-}(X^{2-})_2$.) Some of the examples have a high-temperature pyrite structure.

This is not the place to describe in detail present theoretical ideas concerning the adoption of one structural type over another. However, considerable debate has centered around the role of secondary metal–metal interactions via d orbitals not directly involved in M–X σ bonding. As we mentioned above, the movement of the metal atoms in the ReS_2 structure is attributed to the formation of cation–cation bonds by this d^3 metal. (Similar types of distortions are found in a variety of other systems; d^1 VO_2, for example, undergoes a phase change associated with the movement of the metal ions together across an octahedral shared edge of the rutile structure.) Similarly it has been suggested (*2*) that distortion of the normal marcasite structure to that of löllingite (d^2 and d^4 cation configurations) via that of the arsenopyrite structure (low-spin d^5) is understandable simply in terms of the occupation of one of these MX σ nonbonding orbitals which points directly toward an adjacent metal atom. Note, however, that our sorting of these structures relies on the fact that there are no d^2 or d^4 pyrite examples, but grossly sorts the d^5 arsenopyrites from the d^5 pyrites because of different ΔE values. The three pyrite examples are high-spin rather than low-spin systems but the indices of our map have no knowledge of this of course. The importance of such direct M–M interactions is to be questioned after numerical calculations (*25*) of the size of the interactions. We recently suggested that löllingite, arsenopyrite, and pyrite systems may be best regarded as 12-, 13-, and 14-electron systems (where we count only the x atom localized electrons) just as the MoS_2, CdI_2, or TiO_2 types were described above as 16-electron systems. The actual description of the system will then again depend crucially upon the difference in orbital energy between metal and ligand, i.e., on ΔE.

We also note a fairly sharp cutoff between the structures with universal dimers $M(X_2)$ and the $NbAs_2$ type where only half of the anions are involved in dimers, between 16 and 17 electrons. At the intersection of the $ZrSi_2$ (half the anions involved in chains), $NbAs_2$ (half the anions involved in pairs), and CdI_2 (no anion–anion interactions) regions we find the $PbCl_2$ structure with rather long anion–anion distances, and the $TiAs_2$ type which geometrically approximates to an equal mixture of $PbCl_2$ and $NbAs_2$ types. This results in one out of four of the crystallographically distinct anions being involved in the formation of pairs. The one example of the MoP_2 structure (MoP) appears in the middle of the $NbAs_2$ field. WP_2 adjacent to it adopts this structure at higher temperatures. Hulliger has suggested that it is an impurity-stabilized phase (*2*). Interestingly the $PbCl_2$ type may be regarded (*20*) as a distorted rutile (or CdI_2) type, relationships in keeping with its location on our map.

The $CuAl_2$ type is not well sorted on our map. Apart from two examples found in the $NbAs_2$ region (VSb_2, $TiSb_2$) this type is found in close association with the CaF_2 arrangement. These two structural types are readily derived from the CsCl structure as shown in Table I. In the $CuAl_2$ arrangement the 4^4 nets (C) of the primitive cubic geometry are distorted to give 3^2434 nets of different orientations (A,A',B,B'). Stacking of a upon A' leads to square antiprismatic voids at the cell center and corners. Stacking of C-type nets leads to cubal voids which are all filled in the CsCl structure, and half-filled in the CaF_2 structure, etc. Of interest

TABLE I

Stacking sequence[a]	Example
$C1$	CsCl
$C\frac{1}{2}$	Not known
$C\frac{1}{2}C\frac{1}{2}'$	CaF_2
$A'1A1$	$CuAl_2$ (simple distortion of $C\frac{1}{2}$)
$A'1A1$ + centered diamonds	TlSe (simple distortion of $C1$)
$C1C0$	$FeSi_2$
$1A'1C1B1C$	$CoGe_2$
$A1C1B1C1A'1C1B'1C1$	$PdSn_2$
$1A'0A$	$PtPb_4$
$1AB'1BA''$	$PtSn_4$

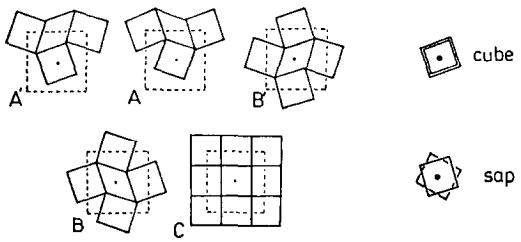

[a] In $XnYm$, n,m represent the fraction of cubal or square antiprismatic holes occupied in the structure formed by stacking X,Y nets on top of each other.

are the borderline locations of the $CoGe_2$ and $PdSn_2$ structures (Table I) on the map, sandwiched between $CuAl_2$ and CaF_2 examples. $RhSn_2$ has the $CuAl_2$ structure at high temperature and a complex one at low temperature. The latter can be described as being made up of two $CuAl_2$-type slabs alternating with a CaF_2-type slab.

Of particular interest is the central position of $FeSi_2$, which is found as a unique structure type (Table I) based also on the CsCl structure. It is also known in the $NbAs_2$ structure and examples of this arrangement lie close by. It is also related in a simple way to the $MoSi_2$ type, another adjacent field in Fig. 1. Whereas $MoSi_2$ was earlier described as being related to the NaCl structure by replacement of the nonmetal by Si_2 pairs parallel to 001, the $FeSi_2$ structure results from a similar replacement in CsCl. The borderline between the $CuAl_2$/CaF_2 and the pyrite/marcasite region is an interesting one too. $AuSn_2$ lies here and it has an unusual structure. Isotypic with the brookite variant of TiO_2 it can be regarded as containing very rumpled 3^2434 nets of Sn atoms stacked on top of each other to give distorted cubal voids. However, it can also be looked at as being made up of slabs of pyrite structure (parallel to 001 planes) with Au sitting in the Fe sites. After two layers of pyrite-like structure, the next slab is oriented in a different way to the one beneath it. Recall also that the fluorite structure is readily derived from that of pyrite by moving the X atoms of the dimers apart. So here with the structure of $AuSn_2$ is an example intermediate between those of $CuAl_2$ and pyrite with similarities to CaF_2.

The rather ill-defined region occupied by $CuAl_2$ merges with the AlB_2 region. There are close similarities here too. $CuAl_2$ contains 3^2434 sheets of X atoms alternating with $\frac{1}{2} \cdot 4^4$ sheets of M atoms; AlB_2 contains 6^3 sheets of X atoms alternating with 3^6 sheets of M atoms. The two are related by simple distortions of both sheets.

$PtGe_2$ with the $CaCl_2$ structure is found on the same $CuAl_2/CaF_2$ borderline with pyrite/marcasite as $AuSn_2$. It is related to the first pair of structures in that half of the holes between adjacent 3^6 sheets of X atoms are filled with metal atoms. Its resemblance to marcasite arises via the approximate hexagonal close packing of the anions in the latter structure. Finally, we note that a rather ill-defined $CuAl_2$ region is also found in transition metal–transition metal maps (*9*).

The geometrical changes as the map is traversed are not, in general, particularly abrupt. Structural related systems are invariably next to each other, although the dividing lines are sometimes fuzzy. In particular it is interesting to note the borderline occurrence of polymorphic systems and the observation sometimes of rather complex structures (e.g., $CoGe_2$) which have fea-

tures of two structural types close by. (There are unusual features too which we haven't mentioned: the Mg_2Cu structure of $NbSn_2$, the occurrence of the Cu_2Sb structure type, and of examples with the PbFCl arrangement.) Clearly the construction of such a map aids our organization of such species in a pedagogic sense and this is our major aim here.

The MX Series

The structural map shown in Fig. 3 separates quite well the CrB (and related types), NiAs (and related types), FeSi, CsCl, and NaCl structures. The related CrB and FeB examples are not well sorted within their field. Within the NiAs region, its orthorhombically distorted variant MnP is found primarily in an area in the middle. This is particularly interesting since the NiAs phases usually extend over a compositional range and the 1 : 1 compound in many cases has a different structure. (We used the Landolt–Börnstein tabulation (*4*) as our arbiter here). The structurally closely related MoP (WC type), NbAs, and TiAs structures are found grouped together within the larger NiAs field. The TiAs structural examples are found right at the boundary with the NaCl structure. This is nicely in keeping with its structure. The anion stacking in NaCl is 100% cubic, i.e., *ccc*. In NiAs, it is 100% hexagonal, *hh*, and in TiAs an equal mixture, namely, *hchc*. So this structure contains half the metal atoms in octahedral and half in trigonal prismatic coordination. ZrP right at the boundary is reported in both TiAs and NaCl structure types. Another group of examples at the edge of the NiAs field but with a larger number of electrons have the millerite (NiS) structure. CoS, NiS, and CoSe are also known in the NiAs structure.

At the bottom of the NiAs field is also found the unusual PbO structure for FeS (also known in the NiAs structure) and FeSe. Here too are the ZnS structures of MnS and MnSe. (MnTe is found both in the NiAs and NaCl structure types.) To the far right lie the PtS (cooperite) and CuS (covellite) structural examples.

Most of the polymorphic examples lie in positions in keeping with the features of the structure map. At the top of the diagram, the boundary NiSi and RhSi examples are known in both FeSi and MnP structures, PdAl is found in both FeSi and CsCl arrangements, and NiIn is known in both CsCl and CoSn forms. Two exceptions are RuSi and OsSi, both with low-temperature FeSi structures. Both are located in the middle of the FeSi field but have higher-temperature CsCl variants.

Of interest is the relationship of this map to the MX_2 map of Fig. 2. The CsCl structure occupies the same region in MX as the related CaF_2 and $CuAl_2$ types do in MX_2. The CrB and FeB region extends over the area occupied by AlB_2 and $ZrSi_2$. All four structure types are dominated by trigonal prismatic metal coordination. The NiAs structure is simply a filled-up CdI_2 type and there is an area of overlap of the MX NiAs and MX_2 CdI_2 fields. For many of these M/X pairs in this region a wide range of species are known between MX and MX_2 stoichiometries as the CdI_2 structure is gradually filled up. Most of the CdI_2 field and all of the rutile field in MX_2 is occupied by that of rock salt in MX, a cubic rather than hexagonal close-packed structure. For some species there seem to be direct mapping relationships. One example is the simple relationship between $PdBi_2$ and CoGe, two structures each represented on the maps by a single example. $PdBi_2$ is directly reached from CoGe by leaving out all of the octahedrally coordinated metal atoms, in a similar way to the derivation of CdI_2 from NiAs. It is interesting that both species have very similar ΔE values and the numbers of electrons per atom (5.5 and 6.0) are

close in the two compounds. For some other systems where the M,X site occupancies are not so directly related the structural pairs occur in different regions on the two maps. One example is the pair FeSi/pyrite. FeSi may be regarded as a defect derivative of pyrite where Fe and Si occupy the X_2 pyrite sites and the M atom is left out.

Watson and Bennett (*8*) have presented a structure map for some of these MX systems. They only included MnP, NiAs, CrB, CsCl, FeSi, and NaCl structure types in their data base. Their indices were an electronegativity difference, much after the style of our ΔE, and the valence s,p energy separation on the X atom. The importance of the latter in providing good sorting diagrams is well established since the early work of St. John and Bloch (*6*), especially for octet systems. Our map is interesting in that only one of the indices (ΔE) is dependent on both the row and column numbers of each atom. The other (N) is simply dependent on the column number. In this light it is interesting to note than an identically defined ΔE versus N display for transition metal–transition metal compounds sorts these alloys well (*27*). The maps are in fact very similar to Watson and Bennett's alloy maps (*9*), where a "ΔE" and "N" are extracted from the band structures of the elemental metals. By way of contrast, alloy maps which do not use the electron count (or some similar direct measure of column number) as an index are rather poor (*14, 15*). The crucial dependence of transition metal elemental structure type of d electron count is now well established (*28*).

The location of the boundary lines between structure types will provide a theoretical challenge for some time to come. Preliminary results from band structure calculations (*29*) do indicate, however, that the positive slope of, for example, the FeSi/CsCl and FeSi/MnP boundary lines are reproducible by numerical calculation.

Appendix (*30*)

Data bases used in the construction of Figs. 2 and 3 are collected from Ref. (*1–4*). The letters correspond to those used in the relevant figure.

MX_2

A. Rutile type
FeF_2, PtO_2, MnF_2, IrO_2, RhO_2, CrF_2, OsO_2, RuO_2, $CrCl_2$, VF_2, ReO_2, TcO_2, MnO_2, TiF_2, CrO_2, WO_2, MoO_2, VO_2, TaO_2, NbO_2

B. $IrSe_2$ type
$IrSe_2$, IrS_2 $RhSe_2$

C. CdI_2 type
$FeCl_2$, $FeBr_2$, FeI_2, PtS_2, $PtSe_2$, VCl_2, VBr_2, VI_2, $TiBr_2$, $TiCl_2$, TiI_2, VSe_2, $PtTe_2$, $MnCl_2$, $MnBr_2$, MnI_2, $IrTe_2$, HfS_2, $HfSe_2$, $HfTe_2$, ZrS_2, $ZrSe_2$, $ZrTe_2$, TiS_2, $TiSe_2$, $TiTe_2$

D. Marcasite type
$NiAs_2$, $NiSb_2$, $RuSb_2$, FeS_2, $FeSe_2$, $FeTe_2$, $CoSe_2$, $CoTe_2$, $CuSe_2$

E. PdS_2 type
PdS_2, $PdSe_2$

F. Löllingite type
FeP_2, $FeAs_2$, $FeSb_2$, RuP_2, $RuAs_2$, $RuSb_2$, OsP_2, $OsAs_2$, $OsSb_2$, $CrSb_2$

G. Pyrite type
NiS_2, $NiSe_2$, $NiTe_2$, RhS_2, CoS_2, OsS_2, $OsSe_2$, $OsTe_2$, RuS_2, $RuSe_2$, $RuTe_2$, PtP_2, $PtAs_2$, $PtSb_2$, $PtBi_2$, $PdAs_2$, $PdSb_2$, MnS_2, $MnSe_2$, $MnTe_2$, $RuSn_2$, $CuTe_2$, CuS_2, $AuSb_2$, $PdBi_2$

H. $HfGa_2$ type
$HfGa_2$, $TiGa_2$, $TiAl_2$, $ZrIn_2$

I. CuP_2 type
CuP_2, AgP_2

J. $MoSi_2$ type
$ReSi_2$, WSi_2, $MoSi_2$, $MoGe_2$, $OsAl_2$

K. PdP_2 type
PdP_2, PtP_2

L. ReS_2 type
ReS_2, $ReSe_2$

M. Arsenopyrite type
FePS, FeAsS, FeSbS, FePSe, FeAsSe, FeSbSe, FeAsTe, FeSbTe, RuPS, RuAsS, RuSbS, RuPSe, RuAsSe, RuSbSe, RuAsTe, RuSbTe, OsPS, OsAsS, OsSbS, OsPSe, OsAsSe, OsSbSe, OsBiSe, OsAsTe, OsSbTe, OsBiTe, IrP_2, $IrAs_2$, $IrSb_2$, $IrBi_2$, $CoAs_2$, $CoSb_2$, RhP_2, $RhAs_2$, $RhBi_2$, $RhSb_2$

N. $AuSn_2$ type
$AuSn_2$

O. $CuAl_2$ type
$CuAl_2$, $AuPb_2$, $PdPb_2$, $RhPb_2$, $CoSn_2$, $AgIn_2$, $FeGe_2$, $FeSn_2$, VSb_2, $MnSn_2$, $TiSb_2$

P. MoS_2 type
MoS_2, $SrCl_2$, $ZrBr_2$, ZrI_2, WS_2, $MoTe_2$, WSe_2, WS_2, WTe_2

Q. $PdSn_2$ type
$PdSn_2$, $CoGe_2$ (related structures, see Table I)

R. CaF_2 type
$PtSb_2$, $NiSi_2$, $IrSn_2$, $CoSi_2$, $NiGa_2$, $NiAl_2$, $NiIn_2$, $PtGa_2$, $PtAl_2$, $PtIn_2$, HfO_2, ZrO_2

S. MoS_2 and CdI_2 type
TaS_2, $TaSe_2$, NbS_2, $NbSe_2$

T. $NbAs_2$ type
$NbAs_2$, $TaTe_2$, $NbTe_2$, WP_2, WAs_2, $MoAs_2$, CrP_2, $CrAs_2$, $OsGe_2$, $RuGe_2$, TaP_2, $TaSb_2$, $TaAs_2$, NbP_2, $NbSb_2$, VP_2, VAs_2

U. $PbCl_2$ type
TiP_2, HfP_2, $HfAs_2$, ZrP_2, $ZrAs_2$, YS_2

V. $TiAs_2$ type
$TiAs_2$, YSe_2, $HfSb_2$, $HfBi_2$, $ZrSb_2$, $ZrBi_2$

W. $CrSi_2$ type
$CrSi_2$, $TaSi_2$, $NbSi_2$, $TaGe_2$, $NbGe_2$, VSi_2

X. $CuMg_2$ type
$NbSn_2$

Y. $TiSi_2$ type
$TiSi_2$, $TiGe_2$, $ZrSn_2$, $RuAl_2$, $RuGa_2$

Z. $ZrSi_2$ type
$ZrSi_2$, $HfSi_2$, $HfGe_2$, $ZrGe_2$, YSn_2

a. $GdSi_2$ type
YSi_2

b. Cu_2Sb type
$LaSe_2$, $LaTe_2$

c. $\alpha ThSi_2$ type
$LaSi_2$, $LaGe_2$, YGe_2

d. $CaCl_2$ type
$PtGe_2$

e. Cu_2Mg type
$LaAl_2$, $ScAl_2$, YAl_2

f. RuB_2 type
RuB_2

g. ReB_2 type
ReB_2, TcB_2

h. CaC_2 type
LaC_2, YC_2

i. MoP_2 type
MoP_2

j. AlB_2 type
CrB_2, HfB_2, LaB_2, MnB_2, MoB_2, NbB_2, OsB_2, ScB_2, TaB_2, TiB_2, VB_2, WB_2, YB_2, ZrB_2

k. $MgZn_2$ type
$ZrAl_2$, $HfAl_2$

l. $ZrGa_2$ type
$ZrGa_2$

m. $FeSi_2$ type
$FeSi_2$

n. PbFCl type
YSbSe, YSbTe, ZrSiS

o. $AuTe_2$ type
$AuTe_2$

p. $PdBi_2$ type
$PdBi_2$

q. Chimney-ladder structures
Mo_6Ge_{16}, $Mo_{13}Ge_{23}$, Tc_4Si_7, $Cr_{11}Ge_{19}$, $Mn_{11}Si_{19}$, $Mn_{15}Si_{26}$, $Rh_{10}Ga_{17}$, Ir_3Ga_5, Ru_2Sn_3, $Rh_{17}Ge_{22}$, Ir_4Ge_5

MX

A. CsCl type
ScAl, CoGa, FeAl, FeGa, LaIn, IrAl, IrGa, LaTl, MnIn, NiAl, NiGa, NiIn, OsAl, OsSi, PdAl, PdIn, ReAl, RhAl, RhGa, RhIn, RuAl, RuGa, YIn, YTl, CoAl, RhSi, OsSi, RuSi, NiIn, YAl, PdAl

B. NiAs type
AuSn, CoS, CoSb, CoSe, CoTe, CrS, CrSb, CrSe, CrTe, CuGe, CuSn, FeS, FeSb, FeSe, FeSn, FeTe, IrPb, IrSb, IrSn, IrTe, MnBi, MnSb, MnSn, MnTe, NiAs, NiBi, NiS, NiSb, NiSe, NiSn, NiTe, PdBi, PdSb, PdTe, PtB, PtBi, PtPb, PtSb, PtSn, PtTe, RhBi, RhSe, RhTe, ScTe, TiAs, TiP, TiS, TiSb, TiSe, TiTe, VP, VS, VSb, VSe, VTe, ZrAs, ZrTe, RhB, MnAs, CoAs

C. CuS type
CuS, CuSe

D. AuCd type
TiPb

E. NbPb type
NbPb

F. FeSi type
CoSi, CrGe, CrSi, FeSi, HfSb, HfSn, MnSi, PdGa, PtAl, PtGa, ReSi, RhSn, RuGe, RuSi, TiSi, OsSi, RhSi, FeGe, PdAl, NiSi

G. FeB type
CoB, FeB, HfB, HfGe, HfSi, LaGe, LaSi, MnB, TiB, TiGe, TiSi, ZrGe, ZrSi

H. MnP type
AuGa, CoAs, CoP, CrAs, CrP, FeAs, FeP, IrGe, IrSi, MnAs, MnP, MoAs, NiGe, NiSi, OsAs, OsP, PdGe, PdSi, PdSn, PtGe, PtSi, RhAs, RhGe, RhSb, RhSi, RuAs, RuP, RuSb, VAs, WP, RhSi

I. CrB type
LaAl, YAl, CrB, LaGa, YGa, HfAl, MoB, NbB, NiB, ScGa, ScGe, ScSi, TaB, VB, WB, YGe, YSi, ZrAl, ZrSi

J. CoSn type
CoSn, FeGe, PtTl, FeSn

K. MoP type
MoP, OsC, RuC, TaN, WC, MoC

L. CuAu type
TiAl, TiGa

M. NaCl type
AgBr, AgCl, AgF, LaAs, LaBi, LaN, LaO, LaP, LaS, LaSb, LaSe, LaTe, ScAs, ScBi, SCN, ScP, ScS, ScSb, ScSe, YAs, YBi, YO, YN, YP, YS, YSb, YSe, YTe, CoO, CrN, CrO, FeC, FeO, HfB, HfC, HfN, MnO, MnTe, MoC, NbC, NbN, NbO, NiO, ScC, TaC, TaO, TcN, TiB, TiC, TiN, TiO, VC, VN, VO, WC, WN, ZrB, ZrC, ZrN, ZrO, $ZrP_{0.9}$, ZrS

N. ZnS type
CuBr, CuCl, CuI, MnS, MnSe

O. TiAs type
TiP, HfAs, ZrP

P. NbAs type
TaP, NbP

Q. NiS type
NiS, NiSe, CoSe, CoS

R. CuTe type
CuTe

S. PdS type
PdS, PdSe

T. PtS type
PtS

U. $InNi_2$ type
FeSb

V. CoGe type (Ni_3Sn_4)
CoGe

W. PbO type
FeS, FeSe

Acknowledgments

This research was supported by the National Science Foundation under NSF DMR8019741. I would like to thank H. Itoh, T. J. McLarnan, and S. Lee for many discussions concerning structural relationships between crystal structures, and Judith Curry for writing a structure map generating program.

References

1. W. B. PEARSON, "Crystal Chemistry and Physics of Metals and Alloys," Wiley, New York (1973).
2. E. HULLIGER, *Struct. Bonding* **4,** 83 (1968).
3. W. B. PEARSON, "Handbook of Lattice Spacings and Structures of Metals," Pergamon, Oxford (1967).
4. "Structure Data of Elements and Intermetallic Phases," Landolt–Börnstein, New Series, Vol. 6/III, Springer-Verlag, Heidelberg (1971).
5. See, for example, C. D. Gerlatt, A. R. Williams, and V. L. Moruzzi, *Phys. Rev. B* (in press), and references therein.
6. J. ST. JOHN AND A. N. BLOCH, *Phys. Rev. Lett.* **33,** 1095 (1974).
7. A. N. BLOCH AND G. C. SCHATTEMAN, *in* "Structure and Bonding in Crystals" (O'Keeffe and Navrotsky, Eds.), Vol. I, Academic Press, New York (1981).
8. R. E. WATSON AND L. H. BENNETT, *J. Phys. Chem. Solids* **39,** 1235 (1978).
9. (a) R. E. WATSON AND L. H. BENNETT, *Phys. Rev. B* **18,** 6439 (1978); (b) L. H. BENNETT AND R. E. WATSON, *in* "Theory of Alloy Phase Formation" (L. H. Bennett, Ed.), Metallurgical Society of AIME, Warrendale, Pa. (1980).
10. E. S. MACHLIN, T. P. CHOW, AND J. C. PHILLIPS, *Phys. Rev. Lett.* **38,** 1292 (1977).
11. J. C. PHILLIPS, *Comments Solid State Phys.* **9,** 11 (1978).
12. A. ZUNGER, *in* "Structure and Bonding in Crystals" (O'Keeffe and Navrotsky, Eds.), Vol. I, Academic Press, New York (1981).
13. A. ZUNGER, *Phys. Rev. B* **22,** 5839 (1980).
14. A. ZUNGER, *Phys. Rev. Lett.* **44,** 582 (1980); **47,** 1086 (1981).
15. E. S. MACHLIN AND B. LOH, *Phys. Rev. Lett.* **45,** 1642 (1980); **47,** 1087 (1981).
16. J. K. BURDETT, G. D. PRICE, AND S. L. PRICE, *Phys. Rev. B* **24,** 2903 (1981).
17. J. K. BURDETT, *Acc. Chem. Res.* **15,** 34 (1982).
18. J. K. BURDETT, *Advan. Chem. Phys.* **49,** 47 (1982).
19. (a) E. MOOSER AND W. B. PEARSON, *Acta Crystallogr.* **12,** 1015 (1959); (b) W. B. PEARSON, *J. Phys. Chem. Solids* **23,** 103 (1962).
20. J. K. BURDETT AND T. J. MCLARNAN, *Inorg. Chem.* **21,** 1119 (1982).
21. J. H. BULARZIK, J. K. BURDETT, AND T. J. MCLARNAN, *Inorg. Chem.* **21,** 1434 (1982).
22. (a) J. K. BURDETT AND T. J. MCLARNAN, *J. Chem. Phys.* **75,** 5764 (1981; (b) J. K. BURDETT, P. HAALAND, AND T. J. MCLARNAN, *J. Chem. Phys.* **75,** 5774 (1981).
23. D. M. P. MINGOS, *Nature (Phys. Sci.)* **236,** 99 (1972).
24. F. HERMAN AND S. SKILLMAN, "Atomic Structure Calculations," Prentice–Hall, Englewood Cliffs, N.J. (1963).
25. See, for example, J. G. NORMAN, B. J. KALBACHER, AND S. J. JACKELS, *J. Chem. Soc. Chem. Commun.* **23,** 1027 (1978).
26. J. A. TOSSELL, D. J. VAUGHAN, AND J. K. BURDETT, *Phys. Chem. Mineral.* **7,** 177 (1981).
27. J. K. BURDETT, unpublished results.
28. D. G. PETTIFOR, *Calphad* **1,** 305 (1977).
29. J. K. BURDETT AND H. ITOH, unpublished results.
30. Landolt–Börnstein list AgB_2 and AuB_2 as having the AlB_2 structure type. Professor O. J. Kleppa has pointed out that there are in fact no compounds present at this metal–boron stoichiometry. These two compounds, if they existed, would lie in the middle of the top fluorite region of Fig. 1, well separated from the other examples with the AlB_2 structure. I am grateful to Professor Kleppa for bringing this to my attention and would be pleased to hear from others who note other nonexistent species plotted.